Structuring Light by Concentric-Ring Patterned Magnetic Metamaterial Cavities
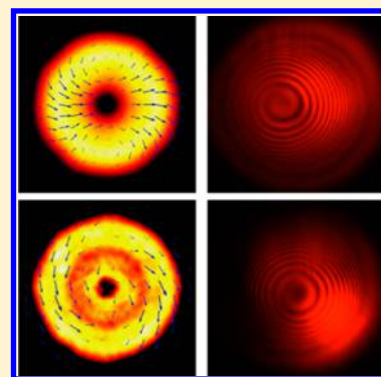
Jinwei Zeng,[†] Jie Gao,[†] Ting S. Luk,[‡] Natalia M. Litchinitser,[§] and Xiaodong Yang*,[†]

[†]Department of Mechanical and Aerospace Engineering, Missouri University of Science and Technology, Rolla, Missouri 65409, United States

[‡]Center for Integrated Nanotechnologies, Sandia National Laboratories, Albuquerque, New Mexico 87185, United States

[§]Department of Electrical Engineering, University at Buffalo, The State University of New York, Buffalo, New York 14260, United States

ABSTRACT: Ultracompact and tunable beam converters pose a significant potential for modern optical technologies ranging from classical and quantum communication to optical manipulation. Here we design and demonstrate concentric-ring patterned structures of magnetic metamaterial cavities capable of tailoring both polarization and phase of light by converting circularly polarized light into a vector beam with an orbital angular momentum. We experimentally illustrate the realization of both radially and azimuthally polarized vortex beams using such concentric-ring patterned magnetic metamaterials. These results contribute to the advanced complex light manipulation with optical metamaterials, making it one step closer to realizing the simultaneous control of polarization and orbital angular momentum of light on a chip.

KEYWORDS: Optical vortex, vector beam, magnetic metamaterial cavity, Pancharatnam–Berry phase optical elements, spin angular momentum, orbital angular momentum

The emergence of optical metamaterials (MMs) and metasurfaces opens new opportunities for manipulating the light beams on the micro- and nanoscale.[1] The metamaterials and metasurfaces are artificial, subwavelength-structured materials with unconventional electromagnetic properties, such as artificial magnetism, anisotropic hyperbolic dispersion, negative index of refraction, and near zero permittivity or permeability.[2−7] By virtue of these extraordinary properties, MMs enable new prospects for tailoring the properties of light beams, including not only intensity profile, but also phase front and polarization properties. These new capabilities may find applications for developing a variety of compact photonic devices and systems, such as optical tweezers or on-chip signal processing systems.[8−15]

Until recently, a majority of the demonstrated nanoscale structured light sources and converters were designed to manipulate either the polarization or the orbital angular momentum (OAM) of a light beam. However, the possibility of manipulating both the OAM and polarization states and, in particular, the possibility of generating azimuthally or radially polarized OAM beams as well as vector vortices with complex hybrid polarization, would open new degrees of freedom for a variety of future nanophotonic applications.[16−20]

The simultaneous change of polarization and phase front can be introduced by transmitting the light beam through an anisotropic and inhomogeneous medium, in which the two originally independent physical characteristics of the beam—the polarization and phase front, or more specifically, the spin angular momentum (SAM) and the OAM—may become intercoupled. A general approach to phase manipulation based on the space-domain Pancharatnam−Berry phase[21,22] was first introduced by Hasman et al. In such so-called Pancharatnam−Berry phase optical elements (PBOEs), the phase change originates from the geometrical phase that accompanies space-variant polarization manipulation rather than from optical path differences like in conventional diffractive and refractive elements.[12,23−25] Scalar and vector vortices with arbitrary OAM can be produced by the specially designed PBOEs including metallic nanorods, V-shaped nanoantennas, and nanogratings, with certain optical axis orientations and patterns.[8−10,12−14,16,20,23,26−29] However, it is still challenging to design structures to generate optical vortex beams with tunable vector polarization, since a specific PBOE structure usually can only generate a particular, predesigned polarization distribution.

In order to realize optical vortices with tunable vector polarization, here we propose and demonstrate magnetic MM cavities that can act as either electrical or magnetic polarizer depending on the light wavelength and MM cavity design.[10,30] Their unique properties are enabled by ring-shaped, metal−
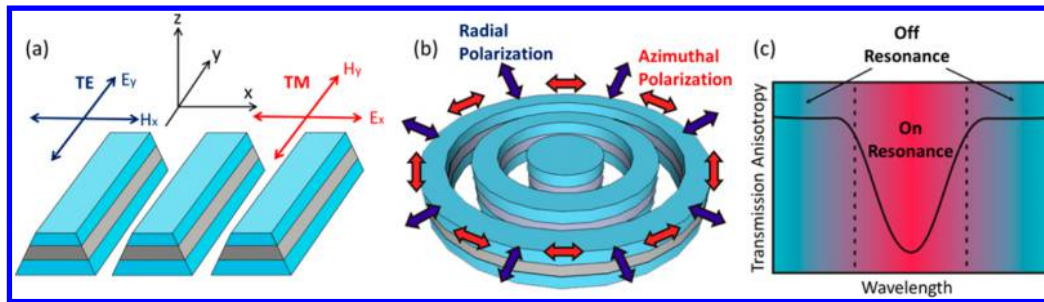
Figure 1. (a, b) Schematics of magnetic MM cavities in straight grating and concentric-ring patterns, respectively. (c) The schematic of transmission anisotropy of typical magnetic MM cavities shows distinct features in off/on-resonance condition.

dielectric−metal MM cavities: at a wavelength corresponding to the magnetic resonance of the three-layer cavity, circularly polarized light is converted into an azimuthally polarized vortex beam; at the wavelength far from the magnetic resonance, the structure acts as a concentric ring based polarizer that was shown to convert a circularly polarized beam into a radially polarized vortex.[11] As a result, properly designed concentric-ring patterned three-layer structures can enable a new way of converting circularly polarized light with a plane wavefront into vector vortex beam with either radial or azimuthal polarization.

In this paper, we fabricate the proposed concentric-ring patterned magnetic MM cavities and demonstrate the possibility of converting the input circularly polarized light into various vector vortex states. The radially polarized vortex beam is generated by the "off-resonance" condition of the magnetic MM cavity, while the azimuthally polarized vortex beam is generated by the "on-resonance" condition. The off- and on-resonance conditions are determined by the light wavelength and the parameters of the concentric-ring patterned structure. As a result, either by changing the operation wavelength, or alternatively, by varying the structural parameters of the magnetic MM cavity, the concentric-ring patterned magnetic MM cavities can be used as efficient SAM−OAM converters that transform the circularly polarized light into an OAM beam with either a radial or azimuthal polarization state.

Here we propose to design the PBOE based on the concentric-ring patterned magnetic MM cavities. Such a device will be shown to convert circularly polarized beam into a vector vortex with either radial or azimuthal polarizations. Figure 1a shows a typical magnetic MM cavity consisting of a pair of metal stripes separated by a dielectric spacer, arranged in a subwavelength periodic array. The physical mechanism of this structure has been extensively studied in previous literature.[3,4,10,30] Under the illumination of transverse magnetic (TM) polarization, where the magnetic field is parallel with the strips, the magnetic field excites a circulating current loop between the top and bottom metal strips around the dielectric spacer, which can induce a magnetic resonance. The magnetic resonance leads to a possibly negative effective permeability, and a transmission minimum near the resonance in the on-resonance condition. Under the illumination of transverse electric (TE) polarization, on the other hand, no optical resonance is supported, and the structure resembles a diluted metal with a generally low transmission. The transmission anisotropy of the structure, which is defined as the transmission of TM-polarized light divided by that of TE-polarized light, will show a high-level flat curve in the off-resonance condition, and exhibit a minimum in the on-resonance condition, as shown in

Figure 1c. As a result, the magnetic MM cavities function as double-axis gratings by exploiting both the electric field and magnetic field of light. In the off-resonance condition, the magnetic MM cavity acts as an electric grating, which blocks the electric field component parallel to the metal stripes; and in the on-resonance condition, the magnetic MM cavity acts as a magnetic grating, which blocks the magnetic field component oriented in parallel with the metal stripes. The location of the resonant wavelength of the magnetic MM cavity is mainly determined by the cavity width, while it has little dependence on the grating period.

As shown in Figure 1b, in order to generate radial and azimuthal polarization distributions, the magnetic MM cavities are arranged in concentric-ring grating patterns such that they would block either the azimuthal polarization component in the off-resonance condition or radial polarization component in the on-resonance condition. Following the PBOE principle, this structure is able to convert a circular polarized beam into an optical vortex beam with either the azimuthal or radial polarization depending on the wavelength.

The basic principle of radial SAM-to-OAM converter can be understood from simple Jones matrix calculations.[10,11] Considering a left-handed (or right-handed) circularly polarized beam, we find that the concentric ring structure would perform the following transformation:

$$
\begin{aligned}
E_{\mathrm{LHC(RHC)}} &= P(r)(e_x + je_y)/\sqrt{2} \\
&= P(r)[(\cos\varphi e_r - \sin\varphi e_\varphi) \\
&\quad + j(\sin\varphi e_r + \cos\varphi e_\varphi)]/\sqrt{2} \\
&= P(r)e^{\pm j\varphi}(e_r \pm je_\varphi)/\sqrt{2}
\end{aligned} \tag{1}
$$

where $P(r)$ and φ represent the amplitude profile and the azimuthal angle in the transverse plane of the incident beam. e_x, e_y, e_r, and e_φ are the unit-vectors in x, y, radial and azimuthal directions. Equation 1 indicates that the output beam acquires a vortex phase (charge +1 or −1) and it may contain both radially and azimuthally polarized components. As discussed above, in the off-resonance state, the transmittance of the radially polarization component is much higher. As a result, a mostly radially polarized vortex beam is expected to be observed at the output end. On the contrary, in the on-resonance state, the magnetic grating will suppress the radial electric field component, resulting in an azimuthally polarized vortex beam at the output end.

In our experiments, a 633 nm HeNe linearly polarized laser was used as the light source, and the magnetic MM cavities with different structural parameters have been designed to make the corresponding on-resonance and off-resonance samples at 633
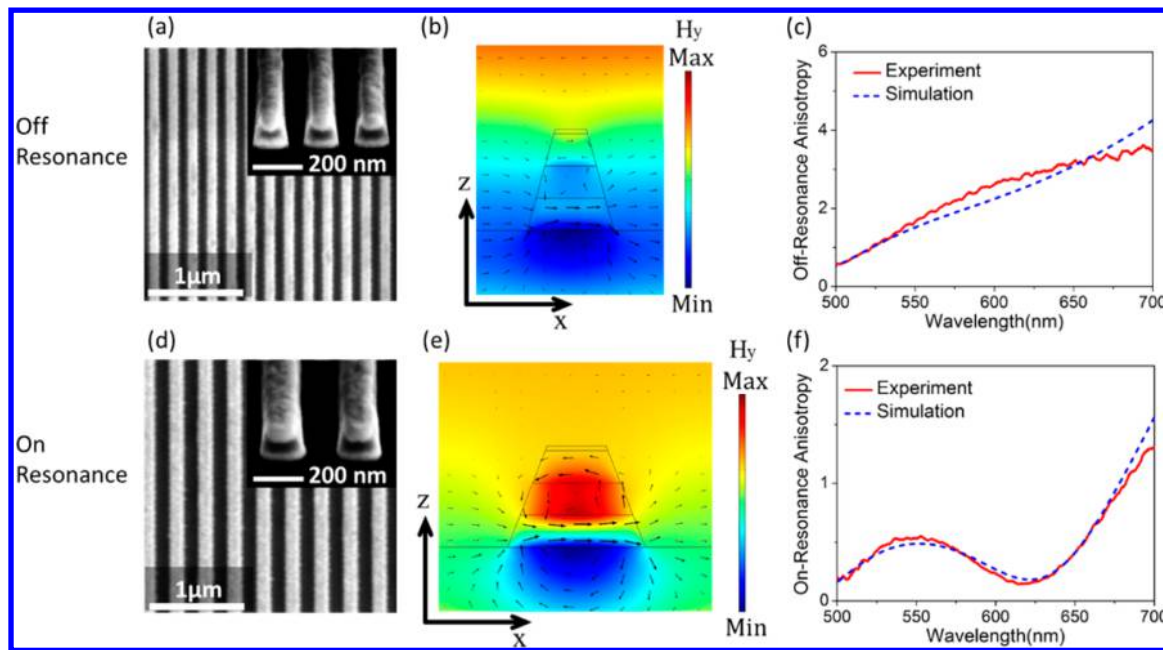
Figure 2. (a, d) The SEM images of the top view and cross-section of the fabricated linear grating magnetic metamaterials. (b, e) The simulated magnetic field and electric displacement distributions under TM polarization, and (c, f) the measured and simulated transmission anisotropy curves of the magnetic MMs cavities in the straight grating patterns.

nm. The three-layer structure consisting of Ag−SiO$_2$−Ag was deposited on the glass slide with the sputtering method, where Ag is deposited at a rate of 0.4 Å/s and SiO$_2$ is deposited at 0.2 Å/s. The thickness of each layer was 40 nm, and a surface protection layer of 5 nm SiO$_2$ was also deposited on top of the three-layer structure. Next, the straight and concentric-ring grating patterns were milled in the multilayers using the focus ion beam (FIB) lithography system. For all of the following experiments, the light beam was always transmitted such that it was entering in the direction from the glass side to the multilayer side.

The magnetic MM cavities with straight grating patterns were fabricated and tested first to confirm that the transmission characteristics of the samples with structural parameters optimized for the off-/on-resonance samples agree with numerical simulation results, and then the same structural parameters were used to design and fabricate concentric-ring cavities. The following optimized structural parameters for the magnetic MM cavities were used: the on-resonance samples had the grating period of 300 nm and the cavity bottom width of 150 nm, while the off-resonance samples had the period of 200 nm and the cavity bottom width of 120 nm. Figure 2a and d show the fabricated straight grating patterns for both the off-resonance and on-resonance samples, and the corresponding measured transmission anisotropy curves are shown in Figure 2c and f compared with numerical simulation results.

The numerical simulations were performed using the finite element method (COMSOL Multiphysics). Based on the SEM image analysis, we measured the side wall angle of the trapezoidal shape of the magnetic MM cavity to be approximately 75° for the off-resonance sample and 70° for the on-resonance sample. The structural parameters of cavity width and period are also obtained from the SEM images. The permittivities of Ag and SiO$_2$ and the film thicknesses in the multilayer structure are characterized with the variable angle spectroscopic ellipsometry (VASE), and the measured values are employed in the simulations. It is noteworthy that the

surface protection layer of 5 nm SiO$_2$ is also included in the simulation. Figure 2b and e shows the magnetic field and polarization distributions in TM polarization at 633 nm. The characteristic feature of the magnetic resonance, a circulating current loop formed between the top and bottom metal strips, can be clearly observed in the case of the on-resonance sample shown in Figure 2e. In contrast, the circulating current loop is the absence in the off-resonance case shown in Figure 2b. The optical transmission spectra through the fabricated samples in the visible range were characterized with a setup including a halogen white light source and a spectrometer to obtain the transmission anisotropy. As shown in Figure 2c and f, the measured transmission anisotropy curves agree well with the simulation results for both the off-resonance and on-resonance samples, which clearly validates our theoretic analysis of the magnetic MM cavity as a double-axis grating controlled by the magnetic resonance.

Based on these structural parameters determined from the analysis of straight grating patterns, the corresponding off-resonance and on-resonance samples of the concentric-ring patterned magnetic MM cavities were fabricated and measured. Figure 3 shows the experimental setup for measuring the optical intensity and phase of the converted beam. The input circularly polarized optical beam from the 633 nm HeNe laser
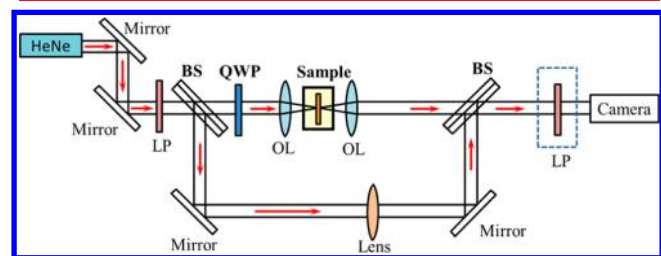

Figure 3. Experimental setup for intensity and phase characterization of the concentric-ring patterned magnetic MM cavities.

was focused onto the sample at normal incidence and the transmitted beam was recollimated with objective lenses. The transmitted beam was then interfered with the linearly polarized spherical reference beam to produce an interference pattern which is conventionally used for the OAM beams characterization.

Figure 4a and d shows the fabricated off-resonance and on-resonance samples of the concentric-ring patterned magnetic
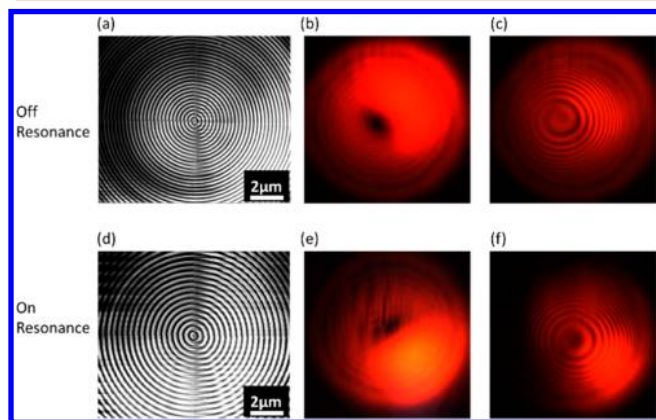

Figure 4. (a, d) The SEM images of the fabricated concentric-ring samples. (b, e) The recorded intensity distributions, and (c, f) the corresponding interference patterns at the wavelength of 633 nm.

MM cavities. During the FIB milling process, each concentric-ring sample was divided into four sections so that the section boundary lines due to slight stitching mismatch can be seen in the SEM images. The intensity distributions of the transmitted beams captured by a CCD camera and interference patterns are shown in Figure 4b, c, e, and f. The intensity distributions found in Figure 4b and d have donut shapes around a dark spot for both the off-resonance and on-resonance samples, while their corresponding interferometry images exhibit single spiral patterns following the same counterclockwise helical orientation. These results demonstrate that optical vortices with the same OAM topological charge of +1 are produced from the left-handed circularly polarized beam for both the off-resonance and on-resonance samples.

The 3D numerical simulations of the concentric-ring patterned magnetic metamaterial cavities were also performed to compare with the experimental data, as shown in Figure 5. In the simulation, the structural parameters of concentric rings were obtained from the SEM image analysis. A circularly polarized plane-wave at 633 nm was incident normally to both the off-resonance and on-resonance samples, and the transmitted fields were calculated. The color maps in Figures 5a and c represent the intensity distributions of the near-field transmitted optical vortex beams, while the arrows represent the polarization distributions. The arrow distributions in a and c clearly show that the beam is radially polarized in the case of the off-resonance sample and azimuthally polarized in the case of the on-resonance sample. As seen in Figure 5b and d, the phase of the corresponding vector polarization changes from $-\pi$ to π in both cases, indicating that the beam possesses the OAM with the topological charge of 1.

Finally, the polarization analysis for the transmitted vector vortices was performed experimentally by placing a linear polarization analyzer right before the CCD camera. As shown in Figures 6 and 7, for both the off-resonance and on-resonance
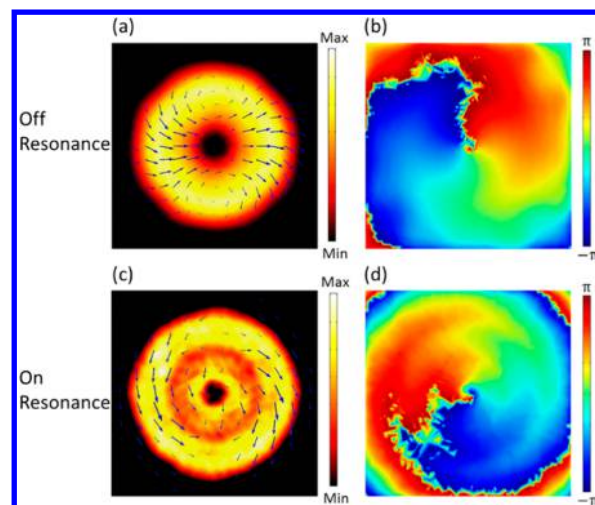

Figure 5. Simulation results of the beam output from the concentric-ring patterned magnetic MMs cavities. (a, c) The intensity and polarization profiles of the transmitted vector vortex beams. (b, d) The phase distributions of the corresponding vector polarization showing the phase variations from $-\pi$ to π.

samples, the transmitted images after passing through the linear polarization analyzer always exhibit two-lobe shapes, rotating with the analyzer rotation. The central dark lines in the off-resonance case are nearly perpendicular to the polarization analyzer axis, signifying the radial polarization of the vortex beam, while the dark lines in the on-resonance case are nearly parallel with the analyzer axis, suggesting the azimuthal polarization of the vortex beam. These experimental results demonstrate the vector polarization distributions, which agree with the simulation results shown in Figure 5a and c.

It is noteworthy that the measured optical vortex images have asymmetric intensity distributions. Besides the deviation between the realistic experiment and the theoretical analysis, a more important reason can be attributed to the limited extinction ratio of the transmission anisotropy for the magnetic MM cavities. According to the PBOE principle, when a circularly polarized beam transmits through perfect linear polarizers, the phase shift difference between two angled polarizers is equal to this orientation angle. However, the magnetic MM cavities in both off-resonance and on-resonance conditions have only limited transmission anisotropy in the fabricated samples, so that the polarization distribution of the transmitted beam is not perfectly linear but elliptical after passing through the polarization analyzer. Therefore, the phase shift difference between the transmitted beams from two angled magnetic MM cavities is less than their orientation angle, causing the overall azimuthal phase gradient induced by the concentric-ring patterned cavities to be marginally less than 2π. Consequently, the generated optical vortex beams have noninteger topological charges of OAM. Previous studies suggest that optical vortices with noninteger charges of OAM are not stable[31] and the singularity is likely to be split by the optical scattering. Each of the split singularities has an integer charge, which makes the overall beam as composite vortices with an asymmetric intensity profile.[32−35] However, this minor intensity asymmetry of the beam can be cleaned afterward as it is done in many structured light experiments.

In summary, we designed and demonstrated the concentric-ring patterned magnetic MM cavities enabling spin-to-orbital angular momentum conversion and generation of vector beams
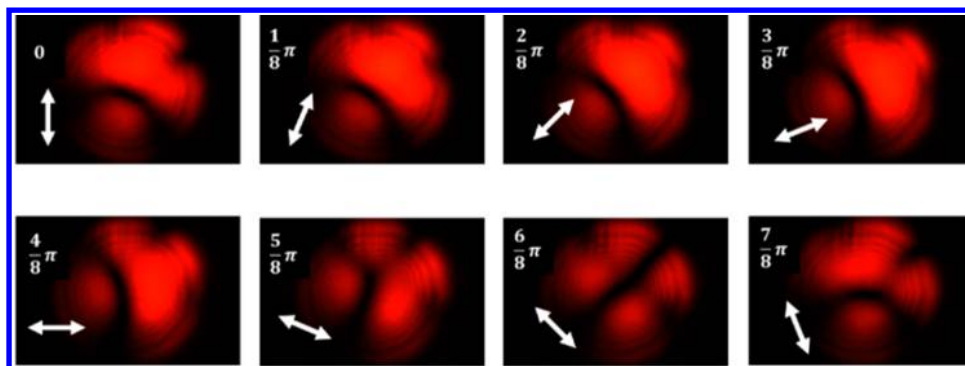
Figure 6. Measured beam intensity profiles after passing through a rotating linear polarization analyzer for the case of the off-resonance sample. The white arrows represent the orientation angles of the analyzer from 0 to $7\pi/8$.
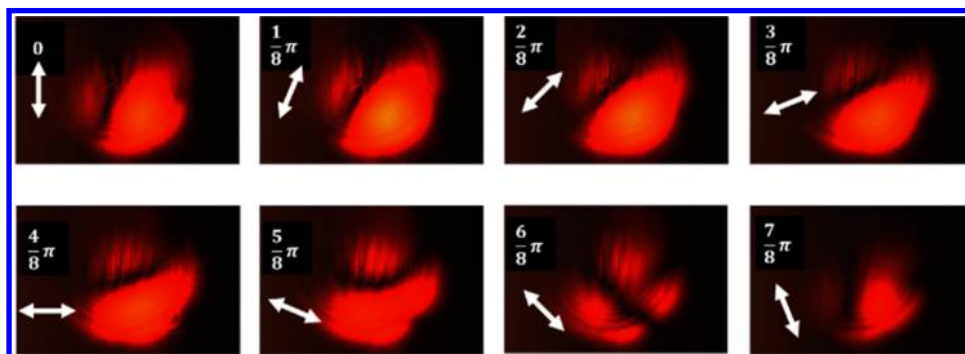

Figure 7. Measured beam intensity profiles after passing through a rotating linear polarization analyzer for the case of the on-resonance sample. The white arrows represent the orientation angles of the analyzer from 0 to $7\pi/8$.

with an OAM. The generated vector polarization states are determined by the frequency of the light beam with respect to the magnetic resonance frequency of the magnetic MM cavity. The vector vortex beams with adjustable vector polarization states may find applications that involve cylindrical waveguides, such as optical fibers, potentially allowing the utilization of both polarization and OAM for high-capacity optical communications. The ultracompact footprint of the proposed device is readily compatible with the future nanophotonics circuits, optical trapping, and manipulation devices.

■ AUTHOR INFORMATION

Corresponding Author
*E-mail: (X.Y.) yangxia@mst.edu.

Author Contributions
The manuscript was written in a collaborative effort from all authors. All authors have given approval to the final version of the manuscript.

Notes
The authors declare no competing financial interest.

■ REFERENCES

(1) Litchinitser, N. M. *Science* **2012**, *337*, 1054−1055.
(2) Yao, J.; Liu, Z.; Liu, Y.; Wang, Y.; Sun, C.; Bartal, G.; Stacy, A. M.; Zhang, X. *Science* **2008**, *321*, 930−930.
(3) Yang, X.; Yao, J.; Rho, J.; Yin, X.; Zhang, X. *Nat. Photonics* **2012**, *6*, 450−454.
(4) Sarychev, A. K.; Shalaev, V. M. *Proc. SPIE 5508, Complex Mediums V: Light and Complexity* **2004**, *128*, 128−137.
(5) Alù, A.; Engheta, N. *Phys. Rev. E* **2005**, *72*, 016623.
(6) Sun, L.; Gao, J.; Yang, X. *Phys. Rev. B: Condens. Matter Mater. Phys.* **2013**, *87*, 165134.
(7) Valentine, J.; Zhang, S.; Zentgraf, T.; Ulin-Avila, E.; Genov, D. A.; Bartal, G.; Zhang, X. *Nature* **2008**, *455*, 376−379.
(8) Sun, J.; Zeng, J.; Litchinitser, N. M. *Opt. Express* **2013**, *21*, 14975−14981.
(9) Sun, J.; Wang, X.; Xu, T.; Kudyshev, Z. A.; Cartwright, A. N.; Litchinitser, N. M. *Nano Lett.* **2014**, *14*, 2726−2729.
(10) Zeng, J.; Wang, X.; Sun, J.; Pandey, A.; Cartwright, A. N.; Litchinitser, N. M. *Sci. Rep.* **2013**, *3*, 2826.
(11) Chen, W.; Han, W.; Abeysinghe, D. C.; Nelson, R. L.; Zhan, Q. *J. Opt.* **2011**, *13*, 015003.
(12) Karimi, E.; Schulz, S. A.; De Leon, I.; Qassim, H.; Upham, J.; Boyd, R. W. *Light: Sci. Appl.* **2014**, *3*, e167.
(13) Yang, Y.; Wang, W.; Moitra, P.; Kravchenko, I. I.; Briggs, D. P.; Valentine, J. *Nano Lett.* **2014**, *14*, 1394−1399.
(14) Yu, N.; Genevet, P.; Kats, M. A.; Aieta, F.; Tetienne, J.-P.; Capasso, F.; Gaburro, Z. *Science* **2011**, *334*, 333−337.

(15) Zhao, Z.; Wang, J.; Li, S.; Willner, A. E. *Opt. Lett.* **2013**, *38*, 932−934.

(16) Niv, A.; Biener, G.; Kleiner, V.; Hasman, E. *Opt. Express* **2006**, *14*, 4208−4220.

(17) Snyder, A. W.; Young, W. R. *J. Opt. Soc. Am.* **1978**, *68*, 297−309.

(18) Volpe, G.; Petrov, D. *Opt. Commun.* **2004**, *237*, 89−95.

(19) Gloge, D. *Appl. Opt.* **1971**, *10*, 2252−2258.

(20) Zhan, Q. *Adv. Opt. Photonics* **2009**, *1*, 1−57.

(21) Berry, M. V. *Proc. R. Soc. London, Ser. A* **1984**, *392*, 45−57.

(22) Berry, M. V. *J. Mod. Opt.* **1987**, *34*, 1401−1407.

(23) Bomzon, Z. e.; Biener, G.; Kleiner, V.; Hasman, E. *Opt. Lett.* **2002**, *27*, 285−287.

(24) Bomzon, Z. e.; Kleiner, V.; Hasman, E. *Opt. Lett.* **2001**, *26*, 1424−1426.

(25) Hasman, E.; Kleiner, V.; Biener, G.; Niv, A. *Appl. Phys. Lett.* **2003**, *82*, 328−330.

(26) Moh, K.; Yuan, X.-C.; Bu, J.; Burge, R.; Gao, B. Z. *Appl. Opt.* **2007**, *46*, 7544−7551.

(27) Lin, J.; Genevet, P.; Kats, M. A.; Antoniou, N.; Capasso, F. *Nano Lett.* **2013**, *13*, 4269−4274.

(28) Li, G.; Kang, M.; Chen, S.; Zhang, S.; Pun, E. Y.-B.; Cheah, K.; Li, J. *Nano Lett.* **2013**, *13*, 4148−4151.

(29) Ghadyani, Z.; Vartiainen, I.; Harder, I.; Iff, W.; Berger, A.; Lindlein, N.; Kuittinen, M. *Appl. Opt.* **2011**, *50*, 2451−2457.

(30) Cai, W.; Chettiar, U. K.; Yuan, H.-K.; de Silva, V. C.; Kildishev, A. V.; Drachev, V. P.; Shalaev, V. M. *Opt. Express* **2007**, *15*, 3333−3341.

(31) Allen, L.; Beijersbergen, M. W.; Spreeuw, R.; Woerdman, J. *Phys. Rev. A: At., Mol., Opt. Phys.* **1992**, *45*, 8185.

(32) Mair, A.; Vaziri, A.; Weihs, G.; Zeilinger, A. *Nature* **2001**, *412*, 313−316.

(33) Galvez, E.; Smiley, N.; Fernandes, N. *Integr. OptoElectron. Devices* **2006**, *613105−613105−8.

(34) Maleev, I. D.; Swartzlander, G. A., Jr *J. Opt. Soc. Am. B* **2003**, *20*, 1169−1176.

(35) Kumar, A.; Vaity, P.; Singh, R. *Opt. Express* **2011**, *19*, 6182−6190.